Atmospheric Chemistry and Physics

Comparison of global inventories of CO emissions from biomass burning derived from remotely sensed data

D. Stroppiana[1], P. A. Brivio[1], J.-M. Grégoire[2], C. Liousse[3], B. Guillaume[3], C. Granier[4,5,6], A. Mieville[4], M. Chin[5], and G. Pétron[6,7]

[1]CNR-IREA, Consiglio Nazionale delle Ricerche – Istituto per il Rilevamento Elettromagnetico dell'Ambiente, Milano, Italy
[2]Joint Research Centre (JRC) of the European Commission, Institute for Environment and Sustainability (IES), Global Environment Monitoring Unit (GEM), Ispra (VA), Italy
[3]Laboratoire d'Aérologie, UMR 5560, Toulouse, France
[4]Service d'Aéronomie/CNRS, Paris, France
[5]NASA/Goddard Space Flight Center, Greenbelt, MD, USA
[6]NOAA Global Monitoring Division, Earth System Research Laboratory, Boulder, CO, USA
[7]University of Colorado, Cooperative Institute for Research in Environmental Sciences, Boulder, CO, USA

Abstract. We compare five global inventories of monthly CO emissions named VGT, ATSR, MODIS, GFED3 and MOPITT based on remotely sensed active fires and/or burned area products for the year 2003. The objective is to highlight similarities and differences by focusing on the geographical and temporal distribution and on the emissions for three broad land cover classes (forest, savanna/grassland and agriculture). Globally, CO emissions for the year 2003 range between 365 Tg CO (GFED3) and 1422 Tg CO (VGT). Despite the large uncertainty in the total amounts, some common spatial patterns typical of biomass burning can be identified in the boreal forests of Siberia, in agricultural areas of Eastern Europe and Russia and in savanna ecosystems of South America, Africa and Australia. Regionally, the largest difference in terms of total amounts (CV > 100%) and seasonality is observed at the northernmost latitudes, especially in North America and Siberia where VGT appears to overestimate the area affected by fires. On the contrary, Africa shows the best agreement both in terms of total annual amounts (CV = 31%) and of seasonality despite some overestimation of emissions from forest and agriculture observed in the MODIS inventory. In Africa VGT provides the most reliable seasonality. Looking at the broad land cover types, the range of contribution to the global emissions of CO is 64–74%, 23–32% and 3–4% for forest, savanna/grassland and agriculture, respec-

tively. These results suggest that there is still large uncertainty in global estimates of emissions and it increases if the comparison is carried by out taking into account the temporal (month) and spatial ($0.5° × 0.5°$ cell) dimensions. Besides the area affected by fires, also vegetation characteristics and conditions at the time of burning should also be accurately parameterized since they can greatly influence the global estimates of CO emissions.

1 Introduction

Since the late 70s, prescribed and wild vegetation fires have been recognized as a major source of atmospheric trace gases and aerosol particles that affect the composition of the atmosphere and the global climate (Crutzen et al., 1979). Fires are a significant anthropogenic source of greenhouse gases (CO_2 and CH_4): deforestation and changing agricultural practices have contributed 25% to the increase in CO_2 since pre-industrial time (IPCC, 2007). Other carbonaceous compounds are also emitted by the incomplete combustion of vegetation such as CO: CO_2 and CO are in fact responsible for 90–95% of the total carbon released by fires (Andreae and Merlet, 2001). According to IPCC (2001) about 40% of the CO annual budget in the atmosphere is due to fires and fires are responsible for almost all of its inter-annual variability (Novelli et al., 2003; van der Werf et al., 2004). For example, the 1997/1998 El Niño event has been linked to

increased fires in the boreal regions and in the tropics and to a strong atmospheric CO anomaly (Langenfelds et al., 2002; Novelli et al., 2003; van der Werf et al., 2004). Moreover, CO is an important sink for hydroxyl radicals (OH) and it is a precursor of ozone (O$_3$) and for these reasons it plays a key role in chemical transport models of atmospheric pollutants (Jain, 2007).

The remaining fraction of total carbon emitted by fires (5%) is released as particulate matter (Reid et al., 2005). Even if lower in percent, these particles have a strong effect on the radiation budget. The aerosols released by the combustion process scatter and absorb incoming solar radiation and change the atmospheric radiation budget (Hobbs et al., 1997; Podgorny et al., 2003) besides their influence on cloud formation and on cloud microphysical processes (Langmann et al., 2009). Black carbon, which constitutes 5–10% of the particle emissions from fires (Liousse et al., 1996; Reid et al., 2005) and has a direct effect on absorbing radiation in the atmosphere, can also reduce albedo when deposited on snow and ice, thus inducing a positive radiative forcing (global warming). Also, land cover change, which is one of the main causes of vegetation fires, itself induces a change of surface albedo.

These are only some of the major and complex processes that impact on the global climate and have been discussed in a number of studies (Innes et al., 2000). Also, climate variability and change itself can influence fire frequency (Westerling et al., 2006). Finally, let us note that recent publications have pointed out that fires can be a source of extremely toxic products such as mercury (Friedli et al., 2009).

Great uncertainty still exists in the assessment of gas and particulate emissions because of the higher temporal dynamic of vegetation fires with respect to other sources such as fossil fuel combustion (Liousse et al., 2004; Langmann et al., 2009); fires vary from place to place and from year to year and are characterized by high seasonality (Anyamba et al., 2003; Hély et al., 2003; Boschetti et al., 2004; Michel et al., 2005). Remotely sensed data potentially have all the characteristics for quantifying seasonal and inter-annual information on the emissions from vegetation fires because of their global and quasi continuous coverage (Cooke et al., 1996; Generoso et al., 2003). Moreover, the high frequency of acquisition of satellite data is particularly suited for compounds such as CO since its average global lifetime in the atmosphere is about two months.

Two approaches have so far been developed to estimate CO emissions from fires. The *bottom-up* approach relies on the model provided by Seiler and Crutzen (1980) and has been widely applied at continental and global scales with various spaceborne sensors (Barbosa et al., 1999; Stroppiana et al., 2000; Conard et al., 2002; Schultz, 2002; Michel et al., 2005; van der Werf et al., 2006; Yan et al., 2006; Konare et al., 2008, Liousse et al., 2010). In this approach, estimates of the surface burned by fires is converted into emitted gases and aerosols with a multiplicative model of parameters which take into account the amount of biomass available for burning, the biomass actually burned by the fire and the amount of gases and aerosols emitted for each unit of burned biomass. These parameters are generally land cover type dependent.

From the late Nineties, inversion models have been developed to derive emissions from CO concentrations measured in the atmosphere (Manning et al., 1997; Bergamaschi et al., 2000; Pétron et al., 2002). Exploitation of remotely sensed concentrations of atmospheric gases is more recent and has rapidly increased with the use of the NASA-MOPITT (Measurements OF Pollution In The Troposphere) instrument (Chevallier et al., 2009; Pétron et al., 2004; Liu et al., 2005; Arellano et al., 2006). The latter is also known as *top-down* approach and consists of estimating carbon surface fluxes from the atmospheric concentrations.

Large differences in both the geographic distribution and temporal dynamics of global and regional CO emission estimates are reported in literature; these differences are primarily due to uncertainties in the input data on burned area and fuel loads (Langmann et al., 2009) and in either modeling or inversion techniques (Pétron et al., 2004).

Recent developments in remote sensing have made widely available global datasets of active fires and burned areas, which can be exploited for the estimation of emission. Active fire counts (the number of active fires per grid cell) have been used for a long time for depicting temporal and spatial patterns of vegetation fires (Cooke et al., 1996; Dwyer et al., 2000) as well as for quantifying the area burned (Giglio et al., 2006). Since active fire mapping relies on the detection of the high thermal emission from the flaming front of the fire, it is an important source of information for the detection of small events and of fires burning below dense canopies. However, active fire mapping is significantly affected by the presence of clouds at the time of observation and is a sample of the total daily fire activity. By integrating the perimeter of the area affected by the fire, a burned area product should provide a better quantification of the area affected by the fire. Burned area mapping is less affected by could cover due to the persistence of the burned signal. However, burned area mapping can be rather difficult over large areas especially where the remotely sensed signal can be confused with other surface targets (e.g. low albedo surfaces such as shadows, water and some types of soil). Since neither active fire counts nor burned area mapping can provide a satisfying global picture of the geographical and temporal variability of vegetation fires, both are still used by the scientific community for the estimation of the emission.

The objective of this paper is to present the comparison of five global inventories of monthly CO emissions from vegetation fires for the year 2003. We named the inventories VGT, ATSR, MODIS, GFED3 and MOPITT after the name of the sensor used to build the dataset. In particular, we aim to highlight similarities and differences in the seasonality and in the geographical distribution of emissions at the global and continental levels and for three broad land cover types: forest,

savanna/grassland and agriculture. The comparison of global inventories of CO emissions from biomass burning is of particular interest for the atmospheric science community since emissions from fires are the least known input to models of atmospheric circulation (Bian et al., 2007).

Despite the large literature on regional estimates, very few studies have attempted so far to compare global datasets of burned areas or pyrogenic emissions from fires and even fewer have specifically addressed the issue of comparing both spatial and temporal distributions (Bian et al., 2007; Jain, 2007; Chang and Song, 2009). The inventories analysed here are derived from different burned area and/or active fire products and satellite sensors; four of them are based on a *bottom-up* approach while a fifth dataset is derived with a *top-down* approach which exploits the concentrations of atmospheric gases as measured by the MOPITT instrument and inverse modelling techniques. We also analyze the distribution of CO sources among forest, savanna/grassland and agriculture land cover classes for the VGT, ATSR and MODIS products. We focused on CO emissions because biomass burning is the major source of this chemical compound in the troposphere. Moreover, CO emissions are often used as a reference for the estimation of other pollutants during the combustion process (Andreae and Merlet, 2001).

2 Data and methods

The five CO inventories (Table 1) can be divided into three categories. In the first category, three inventories (VGT, ATSR and MODIS) were built directly from recent global fire products derived from satellite time series which were processed to map either the occurrence of fire events or the area burned. These inventories used common land cover map and set of biomass densities, burning efficiency coefficients and emission factors. The common land cover map selected for this work is the Global Land Cover 2000 (GLC2000) (Bartholomé and Belward, 2005) built from the 1 km SPOT VEGETATION imagery. The GLC2000 has a spatial resolution comparable to those of the remotely sensed fire information used to build the inventories analysed in this study. Although other land cover maps are available with a finer resolution (e.g. Globcover) we deemed this spatial detail unsuitable for our purposes.

The fourth inventory (GFED3) was also derived from a satellite fire product but with a different set of data for the fuel load, burning efficiency and emission factors. The fifth inventory (MOPITT) was derived from remotely sensed CO observations coupled with an active fire dataset.

2.1 Global CO inventories

2.1.1 The VGT inventory

This inventory was built by the Centre National de la Recherche Scientifique-Laboratoire d'Aérologie (CNRS-

LA) to derive gaseous and particulate emissions for the 2000–2007 period (Liousse et al., 2010). It is based on the L3JRC burned area product (Tansey et al., 2008) derived from the 1 km daily images of the VEGETATION (VGT) sensor onboard the SPOT (Satellite Pour l'Observation de la Terre) satellites. Developed by a consortium of four European research institutions, the Universities of Leicester, Lisbon, Louvain-la-Neuve, and the European Commission Joint Research Centre (EC-JRC), this data set provides the area burned globally on a daily time step for seven years (2000 to 2007) at a resolution of 1 km. A further calibration was applied to the estimated burned area for the *deciduous broad-leaved tree* (GLC03) and the *deciduous shrub cover* (GLC12) land cover classes of the GLC2000. Corrections to the 1 km burned area map derived from L3JRC were based on the analysis of high resolution satellite data (Landsat Thematic Mapper). Monthly CO was estimated for each land cover type using the Biomass Density (BD [kgm-2]), Burning Efficiency (BE [unitless]) and Emission Factor (EF [gCOkg-1]) values reported in Mieville et al. (2010) and Liousse et al. (2010).

2.1.2 The ATSR inventory

This inventory was extracted from the Inventory for Chemistry Climate studies (GICC) produced by the CNRS-SA (Centre National de la Recherche Scientifique-Service d'Aéronomie) and CNRS-LA in the context of the ACCENT-GEIA program (http://www.accent-network.org/). Emissions of several chemical species from biomass burning for the period 1997–2005 have been quantified in three steps (Mieville et al., 2010). First, the Global Burnt Area 2000 (GBA2000) product was used to derive CO emissions for the year 2000. GBA2000 was released by the EC-JRC in partnerships with eight research institutions (Grégoire et al., 2003) and provides the area burned globally, for each month of the year 2000, as derived from 1 km VGT images (Tansey et al., 2004). The resulting emissions from BD, BE and EF described in Mieville et al. (2010) and Liousse et al. (2010) were re-gridded to a 0.5° × 0.5° resolution and used to calibrate, in terms of spatial and temporal distribution of CO emissions, the active fire counts contained in the World Fire Atlas (WFA) product of the European Space Agency (Arino and Plummer, 2001). The WFA provides the geographical location of night-time active fires, detected by the Along Track Scanning Radiometer (ATSR-2) sensor onboard the ERS-2 (European Remote Sensing) satellite, for the period 1995–2002, and by the Advanced Along Track Scanning Radiometer (AATSR) sensor onboard the ENVISAT platform since 2003 (http://earth.esa.int/ers/eeo9/earth_esa.html). It must be noted that the WFA gives access to a long time series, but is restricted to night-time fire events and shows a relatively high level of false detection as demonstrated by Mota et al. (2005). The calibration was carried out separately for three latitudinal bands (−90° S to −15° S; −15° S to 15° N; 15° N to

Table 1. Remotely sensed CO emission inventories considered in this analysis for the year 2003.

Inventory	Fire observations	Global product	EO system	Reference
VGT	Burned area	L3JRC 2000-07[a]	SPOT-VGT	Liousse et al. (2010)
ATSR	Nighttime active fires	WFA 1996-05[b]	AATSR	Mieville et al. (2010)
MODIS	Active fires	MODIS 2001-04[c,d]	MODIS	Chin et al. (2002)
GFED3	Burned area	MODIS 2000-09[e]	MODIS	Van der Werf et al. (2010)
MOPITT	Active fires	WFA 1996-05[b]	MOPITT	Pétron et al. (2004)

[a] Tansey et al., 2008; [b] Arino and Plummer, 2001; [c] Justice et al., 2002; [d] Giglio et al., 2006; [e] Giglio et al., 2006.

90° N) based on the assumption that within the same latitudinal band and vegetation class all fire pixels of the WFA product represent the same average burned surface, and thus the same average emitted CO. Finally, the WFA time series of night-time fire counts was translated into CO emissions for the 1997–2005 period using the same set of coefficients as the VGT inventory.

2.1.3 The MODIS inventory

This inventory is based on the 8-day fire counts at 1-km resolution derived from the MODIS (Moderate Resolution Imaging Spectroradiometer) sensor onboard the Terra and Aqua satellites (Justice et al., 2002). It uses the Version 4 of the monthly Climate Modeling Grid (CMG) (NASA/University of Maryland, 2002) fire product at $0.5° \times 0.5°$ resolution, from January 2001 to December 2004. The conversion factors proposed by Giglio et al. (2006) were used to build a set of monthly burnt area estimates for the year 2003 (Chin et al., 2002). The MODIS CO inventory was finally derived using the same coefficients as the VGT and ATSR inventories and reported in Mieville et al. (2010) and Liousse et al. (2010).

2.1.4 The GFED3 inventory

The Global Fire Emissions Database version 3 (GFED3) recently released (van der Werf et al., 2010), provides emissions from biomass burning at $0.5° \times 0.5°$ spatial resolution and a monthly time step globally for the period 1997–2009. The source fire information is the burned area dataset, which is composed of daily burned area maps derived from 500 m MODIS data (Giglio et al., 2009; Giglio et al., 2010). With respect to the dataset used for the GFED version 2 (Giglio et al., 2006), in the GFED3 burned areas are directly derived from the satellite images and the use of active fire counts is restricted to those cases where the 500 m direct measurements are not available. The fire activity is combined with a global biogeochemical model to describe the vegetation compound. Compared to the previous GFED2 dataset, several changes have been applied to the algorithm for the parameterization of the vegetation. In the GFED3 inventory the emission estimates are generally lower and the differences are more evident at the regional scale rather than at the global

scale; these differences are fully detailed in van der Werf et al. (2010).

2.1.5 The MOPITT inventory

The MOPITT instrument measures the CO content of the troposphere and the emission inventory was built using a *top-down* model (Pétron et al., 2004). A set of a-priori sources of CO emissions was combined with the global chemistry and transport Model for OZone and Related chemical Tracers (MOZART; Horowitz et al., 2003), which is characterized by a $2.1° \times 2.8°$ resolution, to relate perturbations in the CO surface emissions to perturbations in the CO tropospheric amounts for 63 trace gases. This relationship needs to be "inverted" to transform the differences between the observed and the modeled CO distributions into corrections of the specified a-priori CO fluxes (Pétron et al., 2004). The inversion is designed to produce the best linear unbiased estimate of the emissions by solving a weighted least squares problem. The technique is described in detail in Pétron et al. (2002). Inversion is done for fifteen large regions over the globe. The a-priori emissions from technological activities and biofuel use have no seasonality and are based on annual estimates from the EDGAR-3 inventory (Emission Database for Global Atmospheric Research) (Olivier and Berdowski, 2001); the a-priori emissions from biomass burning were derived on a monthly basis from the ATSR fire counts (Pétron et al., 2004). The dataset was interpolated to a resolution of $0.5° \times 0.5°$ to be consistent with the other datasets.

2.2 Inventory comparison

The five inventories are compared over the globe and six continental windows: North America (180–50° W, 30–75° N), Europe (30° W–45° E, 26–71° N), Northern Asia (45–180° E, 26–71° N), South America (117–33° W, 30–50° S), Africa (30° W–63° E, 26° N–50° S) and South East Asia (63–180° E, 26° N–50° S) (Boschetti et al., 2004). We first compare maps of annual CO and totals over geographical areas. Since totals may hide compensation effects (Generoso et al., 2003), we also analyse the spatial agreement of annual totals by computing the coefficient of determination (R^2) by regressing all $0.5° \times 0.5°$ cells (each cell value is the

sum of the monthly 2003 values) of the geographical windows and the globe. We also compare seasonality (month by month emissions) as provided by the five inventories.

A further analysis is carried out only for the VGT, ATSR and MODIS estimates which were made available per land cover type: we look at the distribution of the emissions among three broad land cover types and derived by grouping the GLC2000 classes where fires occur: forest (GLC2000 classes 1, 2, 4, 5, 6, 9), savanna/grassland (GLC2000 classes 11 to 14) and agriculture (GLC2000 classes 16 to 18) (Mieville et al., 2010). Vegetation characteristics, particularly the high variability of the amount of biomass available for burning, can in fact have a significant weight on the distribution of emissions in space and time (Michel et al., 2005).

3 Results and discussion

3.1 Geographical distribution of CO emissions

Maps of CO emissions for the year 2003 from the five inventories are presented in Fig. 1 and annual totals for the continental windows and the globe are summarized in Table 2. In Fig. 1 we also present (lower right corner) the map of agreement, which shows for each $0.5° \times 0.5°$ cell the number of inventories with total CO emissions greater than zero. The global amounts range from about 365 Tg CO (GFED3) to 1422 Tg CO (VGT), with VGT almost two times greater than the second largest value given by MODIS (769.6 Tg CO). Figure 1 clearly depicts the extreme pictures given by VGT, with extensive sources of CO in the Northern Hemisphere, and by both ATSR and GFED3 with the lowest emissions. In the case of ATSR, the lower rate of emission sources can be ascribed to the use of night-time active fires, which represent an under-sampling of the total daily fire activity. In the case of GFED3, the reasons are more difficult to be identified due to the interaction of the estimates of the area burned and fuel consumption. Van der Werf et al. (2010) compared GFED3 to GFED2 and found that changes of these two factors play differently at the regional scale to produce a lower global rate of CO emissions. From the analysis of the GFED2 inventory (data not shown) we hypothesize that the lower estimate of the area burned in GFED3 might play a key role in the reduced estimates of CO. The MOPITT inventory shows the greatest number of $0.5°$ cells with emissions from biomass burning; however, this is due to the original resolution of the product ($2.1° \times 2.8°$), which might bias spatial comparison with the other inventories derived at a higher resolution. This effect is also highlighted in the agreement map of Fig. 1 where grey cells correspond to MOPITT emissions and are widespread over the globe. In the agreement map the blue regions mainly correspond to areas where only VGT and MOPITT have sources of CO emissions from biomass burning; the red regions are instead the areas where all datasets indentify the presence of sources of CO emissions.

With the exception of VGT, estimates compared in this work are within the ranges given by previous studies. The GFED2 dataset (van der Werf et al., 2006) gives for the period 1997–2004 a minimum for global CO emissions from vegetation fires of 337.6 Tg CO in 2000 and a maximum of 592.2 Tg CO in 1998; for 2003 it provides an estimate of 398 Tg CO emitted from biomass burning. Bian et al. (2007) compared six inventories of CO emissions from biomass burning and found annual totals to range between 489 Tg CO and 518 Tg CO. According to IPCC (2001), the contribution from vegetation fires to the CO global budget ranges between 300 and 700 Tg CO/year although this source is recognized as the most variable part of the CO budget. Jain (2007) compared three global burned area datasets (GLOBSCAR, GBA2000 and GFED2) and found the annual CO emissions to be in the range 320.6–390.4 Tg CO/year although the estimates for the year 2000 might not be representative because of a below average fire activity in some regions of the globe (van der Werf et al., 2010).

In all of the northern continental windows VGT shows the greatest annual totals due to the highest rate of emission sources in Alaska, Western and Eastern US, Western Europe and Russia (Fig. 1). Only the VGT inventory identifies boreal fires in Northern Asia as the most important source of CO (39%) with the African contribution ranked second (21%) (Table 2). In North America and Europe the Coefficient of Variation ($CV = \sigma/\mu$) for annual totals is above 145% and it is 88% in Northern Asia mainly due to the contribution of a large area of high CO emissions from VGT (above 0.1 Tg CO/year/$0.5°$ cell) in Siberia. If the VGT inventory is left out from the computation, CV drops to 55%, 61% and 51% for North America, Europe and Northern Asia, respectively. According to the VGT inventory fires in Europe contribute as much as 6% to the global annual emissions of CO from biomass burning whereas the proportion given by the other inventories is 1–2%. Since a large difference exists also between VGT, ATSR and MODIS, which were derived with common parameters, the observed high emissions in VGT are due to an overestimation of the area burned in the L3JRC product. In the northern regions the difference in burned area estimates is amplified by forest fuel loads, which can be more than 20 times greater than the savanna's, and by forest vegetation composition (e.g. the fraction of tree cover), which can favor emissions of incomplete combustion products such as CO. Chang and Song (2009) observed a large difference between estimates of the MCD45A1 (MODIS Collection 5 product) and L3JRC burned area products over the period 2000 to 2007 for northern latitudes and found that, over the years, the greatest difference occurred just for 2003. Despite the large difference of the total CO emissions, some common spatial patterns of high CO emissions can be indetified in Fig. 1 in central and eastern Siberia: south of Lake Baikal and along the border with Mongolia and China.

Table 2. Total CO emissions [Tg] for the globe and the continental windows and the percentage [%] computed with respect to the global totals. MOPITT values are highlighted in grey as it is the only *top-down* model.

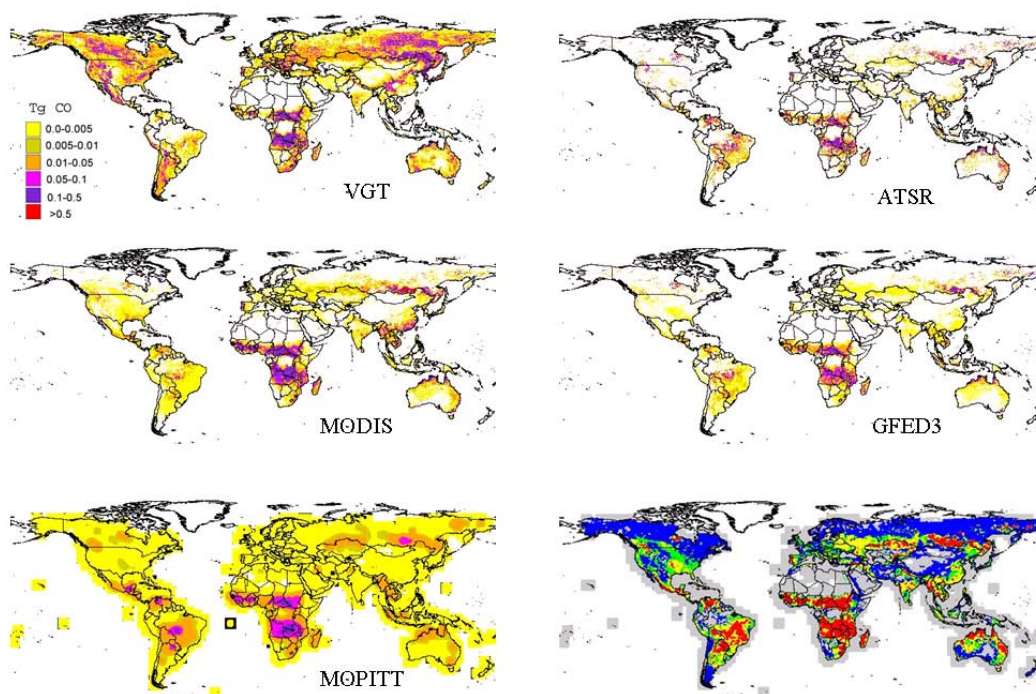|	Total CO [Tg]					Percentage [%]				
	VGT	ATSR	MODIS	GFED3	MOPITT	VGT	ATSR	MODIS	GFED3	MOPITT
N. America	277.6	48.1	19.2	14.8	25.5	19	9	2	4	4
Europe	87.8	7.3	13.2	1.6	9.3	6	1	2	0	2
N. Asia	559.1	139.5	241.6	78.4	102.0	39	25	31	21	17
S. America	121.7	93.1	35.6	53.4	121.9	9	17	5	15	21
Africa	302.7	201.7	367.4	164.7	274.8	21	37	48	45	46
South East Asia	74.0	57.9	92.6	52.6	60.5	5	11	12	14	10
Global	1422.0	547.5	769.6	365.3	594.0	100	100	100	100	100

Fig. 1. Maps of CO emissions [Tg] for the year 2003 for 0.5° grid cells; in the right lower corner the map of agreement (i.e. the number of inventories for each cell with CO emissions greater than zero; grey = 1, blue = 2, green = 3, yellow = 4, red = 5). The agreement map has been filtered with a median filter (3 × 3).

In the southern continental windows the inventories appear to have a more similar geographical distribution of emission sources (Fig. 1). In South America totals from VGT and MO-PITT coincide (121 Tg CO, Table 2) but sources (i.e. fires) are located in different areas of the continent. In fact, VGT shows emissions from the Argentinean savannas whereas all the other inventories agree in pointing out the highest emissions from biomass burning in the savannas south of the Amazonian forest (Fig. 1). Further analyses should be carried out to clearly identify the source of error in the L3JRC burned area dataset, which leads to this overestimation. De-spite the common spatial patterns of emission sources in South America from ATSR, MODIS and GFED3, the total amount can be as low as 35.6 Tg CO as given by MODIS, which represents an underestimation of the total emissions from biomass burning. Giglio et al. (2006) suggested that the quality of the burned area maps over closed canopy forests of South America south of the Equator might have been lowered by cloud and tree canopy covers, which prevents the observation of the surface and affects the mapping of hot spots more than of burned areas.

The inventories best agree over Africa (164.7–367.4 Tg CO, CV = 31%) and South East Asia (52.6–92.60 Tg CO, CV = 24%) where MODIS provides the greatest estimates. The geographical distribution of emission sources is also very similar with three regions of intense burning: Central African Republic, Western Africa and, in the south of the continent, the region encompassing Democratic Republic of Congo, Zambia and Mozambique. Emissions from African vegetation fires cover 37% of the global CO emissions according to ATSR and between 45% and 49% according to GFED3, MODIS and MOPITT inventories. Africa remains a key continent for the global carbon cycle although it accounts for 14% of the global population and only 3% of the global emissions from fossil fuel use (Williams et al., 2007) that increases if regional specificities (biofuel, two wheel emissions ...) are taken into account (Assamoi and Liousse, 2009). In this continent in fact emissions due to biomass burning and land use change are comparable to emissions from fossil fuel use and are not negligible in the total balance (Canadell et al., 2009; Williams et al., 2007). Vegetation fires from southern Africa most contribute to the total continental budget of emitted CO between 54% (MOPITT) and 63% (VGT). Only for the MODIS inventory burning in the northern Africa produces a greater proportion of emissions (52%) with respect to the south (48%). The proportions between north and south are generally the opposite when the area burned, rather than the emissions, is analysed because of the extensive and frequent fires which occur in the Sudania and Guineo-Congolia/Sudania eco-regions; however, the land cover classes affected by fires in the south, more specifically in the Zambezian eco-region, are characterized by greater fuel loads, which result in greater fuel consumption (Roberts et al., 2009). When considering the emissions [Tg CO] for the northern part of the continent, we observe the following ranking in decreasing order: MODIS (191.2), MOPITT (126.4), VGT (112.55), ATSR (89.1) and GFED3 (74.1). For southern Africa, the ranking is: VGT (190.3), MODIS (176.4), MOPITT (148.9), ATSR (112.6) and GFED3 (90.7). Looking at the maps of Fig. 1, the VGT inventory significantly underestimates biomass burning in Western Africa (i.e. along the border between Guinea and Mali) despite the calibration applied for correcting this underestimation by the L3JRC burned area product for GLC2000 classes 3 (*open deciduous broadleaved tree cover*) and 12 (*deciduous closed-open shrubs*). These lower emissions from VGT were observed also by Tansey et al. (2008).

In Africa ATSR shows a lower number of emissions sources although the spatial pattern is similar to that of the other inventories; it is likely that the use of night-time active fires leads to an underestimation of the burned area as a consequence of the strong diurnal cycle of fires (Roberts et al., 2009). Moreover, the temporal sampling due to the short duration of fires is enhanced in the case of polar orbiting satellites, which are characterized by a limited overpass frequency. This is particularly true in the case of savanna fires in Africa which are characterized by a very low temporal persistence (Roberts et al., 2009). Some of the limitations involved in the use of hot spots for emission estimation could be overcome with the Fire Radiative Power (FRP) approach proposed by Wooster et al. (2005). The Fire Radiative Energy (FRE), resulting from the integration over time of the FRP, can in fact be directly linked to the fuel consumption. Moreover, the use of the frequent images from the SEVIRI (Spinning Enhanced Visible and InfraRed Imager) sensor onboard the Meteosat Second Generation (MSG) platform can integrate fire information over the day to reduce the effect of temporal sampling. This approach can be successfully applied for monitoring biomass burning in open vegetation of Africa where fire size and intensity are suitable for the lower spatial resolution of the SEVIRI sensor.

Finally, GFED3 is confirmed to be the lowest estimate among all despite the larger proportion of 0.5° cells with CO emissions greater than zero with respect to, for example, ATSR: indeed most of these cells have low emission values (orange colour key). Previous studies have observed the underestimation of the GFED2 dataset and in particular in tropical areas (Kopacz et al., 2010).

In South East Asia MODIS provides the highest estimates (92.6 Tg CO) followed by VGT (74.0 Tg CO), ATSR and MOPITT with totals around 60 Tg CO and GFED3 (52.6 Tg CO). Chang and Song (2009) found that the L3JRC burned area product underestimates burning in low and sparse vegetation covers of semi-arid Australia but our maps in Fig. 1 show a very similar distribution of CO sources over continental Australia with higher values given by VGT. The greatest total for this window from MODIS is due to emissions in forested regions of Southern China, Myanmar, Cambodia, Northern Laos and Vietnam. GFED3, ATSR and MOPITT have the same geographical distribution but lower emission values compared to MODIS. On the contrary, VGT shows high emissions along the northern border of the Sichuan Basin in China; in this area the evergreen forest is fragmented and mixed with herbaceous vegetation. We think that the L3JRC product might erroneously map as burned some areas covered by herbaceous vegetation. The contribution of South East Asia to the global emissions of CO is not negligible (10–15%) and it can be even more important in terms of burned area for its frequent and extensive fires in tropical savannas (Chang and Song, 2009).

The difference of the spatial patterns of annual CO emissions is quantified by the correlation analysis which compares two inventories at a time (Table 3). The coefficient of determination (R^2) computed between VGT and each of the other inventories is generally the lowest for the northern continental windows and it is null for South America due to the different location of CO sources discussed above. In Europe, Northern Asia, South America, and Africa the greatest correlation is achieved between MODIS and GFED3 ($0.43 < R^2 < 0.71$). In North America the highest R^2 (0.49) is between ATSR and MODIS. In South East Asia the best

Table 3. The coefficient of determination R^2 derived by regressing CO estimates for the 0.5° cells for each window and the globe. In the parenthesis the number of cells used in the regression after discarding cells with zero emissions in both products.

		VGT	ATSR	MODIS	GFED3	MOPITT
N. Am.	VGT	1				
	ATSR	0.04 (9067)	1			
	MODIS	0.08 (9254)	0.49 (3217)	1		
	GFED3	0.03 (9092)	0.24 (1694)	0.31 (3154)		
	MOPITT	0.02 (13 040)	0.05 (12 376)	0.07 (12 371)	0.03 (12 371)	1
Europe	VGT	1				
	ATSR	0.08 (5017)	1			
	MODIS	0.21 (5197)	0.40 (3115)	1		
	GFED3	0.16 (5047)	0.36 (1983)	0.71 (3033)		
	MOPITT	0.05 (10 526)	0.03 (10 448)	0.05 (10 449)	0.03 (10 447)	1
N. Asia	VGT	1				
	ATSR	0.08 (14 112)	1			
	MODIS	0.14 (14 579)	0.38 (6650)	1		
	GFED3	0.16 (14 277)	0.22 (4975)	0.43 (6473)		
	MOPITT	0.10 (19 579)	0.12 (19 331)	0.22 (19 320)	0.18 (19 319)	1
S. Am.	VGT	1				
	ATSR	0.00 (5309)	1			
	MODIS	0.00 (6410)	0.20 (5497)	1		
	GFED3	0.00 (5598)	0.1 (4370)	0.57 (5479)		
	MOPITT	0.00 (13 636)	0.17 (13 625)	0.17 (13 627)	0.08 (13 626)	1
Africa	VGT	1				
	ATSR	0.27 (5100)	1			
	MODIS	0.44 (5895)	0.37 (5290)	1		
	GFED3	0.47 (5455)	0.26 (4668)	0.49 (5255)		
	MOPITT	0.44 (13 634)	0.21 (13 626)	0.47 (13 630)	0.45 (13 625)	1
South East Asia	VGT	1				
	ATSR	0.14 (4401)	1			
	MODIS	0.43 (5567)	0.12 (4613)	1		
	GFED3	0.09 (5007)	0.04 (3660)	0.15 (4562)		
	MOPITT	0.07 (16 257)	0.09 (16 257)	0.05 (16 257)	0.02 (16 257)	1
Global	VGT	1				
	ATSR	0.11 (43 018)	1			
	MODIS	0.20 (46 873)	0.28 (28 255)	1		
	GFED3	0.11 (44 453)	0.13 (21 248)	0.29 (27 812)		
	MOPITT	0.13 (89 275)	0.15 (88 195)	0.21 (88 169)	0.15 (88 160)	1

correlation is between VGT and MODIS ($R^2 = 0.43$). In Africa the similar geographical distribution of emissions shown in Fig. 1 and discussed above is confirmed by the outcome of this analysis of correlation. Note that a greater value of R^2 means a high spatial correlation of the annual totals between two inventories but not necessarily a good agreement in terms of absolute values. Vice versa a good agreement in terms of total emissions might hide a significant difference in the spatial distributions of CO sources such as in the case of South America between VGT and MOPITT (Table 2). However, the regression relationships can be used

for inter-calibration of the products. With the exception of Africa, MOPITT is least correlated to the other inventories as pictured by this analysis.

At the global level, the agreement is very low suggesting that similarities are better highlighted at the regional scale. The maximum R^2 is achieved between MODIS and GFED3 ($R^2 = 0.33$). The MOPITT inventory is best correlated to MODIS and GFED3.
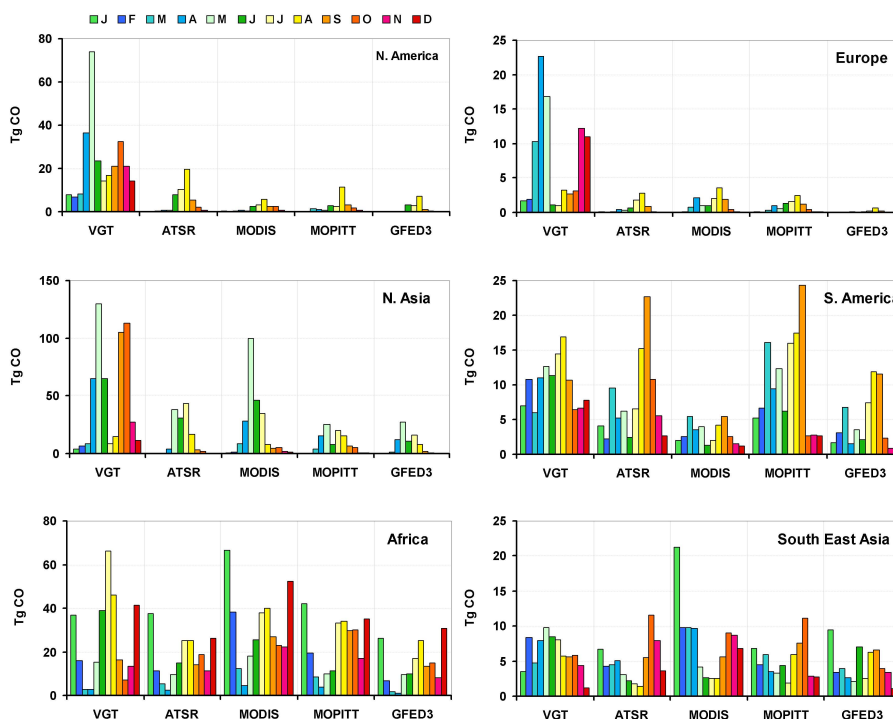
Fig. 2. Seasonality of CO emissions [Tg CO month^{-1}] for each continental window from the five inventories.

3.2 Seasonality of CO emissions

The temporal distribution of monthly emissions (i.e. seasonality) is an important input parameter for both biomass burning studies and models of the circulation of atmospheric pollutants (Kopacz et al., 2010); especially in the case of chemical compounds such as CO which is characterized by a lifetime in the atmosphere of about two months (Crutzen and Zimmermann, 1991).

Figure 2 shows monthly emission estimates given by the five inventories for the continental windows. According to four out of five inventories, in North America fire CO emissions start in June and last four/five months until September/October; the season peak occurs in August with an amount of emitted CO which varies largely: 19.1, 4.8, 7.0 and 11.3 Tg CO according to ATSR, MODIS, GFED3, and MOPITT, respectively. VGT shows emissions throughout the year with peaks in May (73.9 Tg CO) and October (32.6 Tg CO) although emissions in August are in the range of the other inventories (16.6 Tg CO). In Europe, emissions are observed from the ATSR, MODIS and MOPITT inventories from June to September with a first peak in spring (April) and a second one in summer (August); absolute values of emissions are low with summer maxima below 4 Tg CO. In agreement with the other inventories, VGT identifies spring emissions from biomass burning although somewhat overestimated (22.7 Tg CO) and it alone shows fire activity at the end of the year (November and Decem-

ber); in these two months 67% and 73% of the emitted CO comes from fires in *closed deciduous broadleaved forests* (GLC2000 class 2). In Northern Asia emissions last from February/March until September/October. In this window seasonality has the largest variability among the five inventories. In May 2003, the VGT and MODIS inventories show a large area of biomass burning in a belt spanning from European Russia through north Kazakhstan and Mongolia to the Far East of Siberia leading to a total amount of CO emissions in the range 100–130 Tg CO which was also observed by other studies relying on ground measurements and satellite observations (Edwards et al., 2004; Yurganov et al., 2005; van der Werf et al., 2006). These emissions mainly come from biomass burning in *closed deciduous broadleaved forest* (GLC2000 class 2) and *needle-leaved deciduous forest* (GLC2000 class 5). Yet VGT only maps sources of CO in *closed deciduous broadleaved forests* in Eastern Siberia north of this belt, this contribution leads to a higher monthly total. The other inventories show the same area of high CO emissions in the Far East but they underestimate biomass burning in European Russia and along the border between Russia and Kazakhstan where extensive agricultural areas are located. In agricultural lands the use of active fires leads to the under-sampling of the daily fire activity since controlled fires are quick and often extinguished at night. ATSR, MOPITT and GFED3 show emissions in June/July comparable to their same levels in May. The MOPITT inventory shows the same belt of biomass burning sources as VGT

and MODIS although the original resolution of the product ($2.1° \times 2.8°$) makes the spatial comparison less reliable. In Northern Asia only VGT is characterized by a second peak in September/October when the other inventories detect very low emissions.

VGT emissions are of one order magnitude greater compared to the other inventories in Europe and Northern Asia with 22.7 and 12.3 Tg CO in April and November and 129.8 and 113.4 Tg CO in May and October, respectively. It is accepted that the L3JRC product overestimates burned areas and therefore emissions at the northernmost latitudes especially outside the fire season (Chang and Song, 2009). In particular, the effect of snow melting in spring and vegetation senescence in autumn (yellowing and falling leaves) on the spectral signal may have led to mistakenly mapped burned areas. The fact that CO sources in the VGT inventory for the northern continental windows are located in land cover classes of deciduous forests reinforces this hypothesis. However, field data would be necessary to confirm it. The validation exercise carried out by Tansey et al. (2008) does not provide accuracy outside the fire season and the authors themselves suggest a careful use of this data in off-season time.

In the southern windows, the seasonal distribution of monthly emissions is much more similar among the inventories. The best seasonal agreement is reached for Africa: the greatest emissions during the Northern and Southern burning seasons appear clearly from Fig. 2 in December/January and July/August, respectively, for all inventories. However, VGT provides the greatest estimates in July (66.1 Tg CO) due to fires mapped in southern savannas where the other inventories seem to underestimate. The other inventories have the greatest monthly emissions in December and January due to fires in the northern savanna belt. In these two months, the MODIS inventory, for example, has significant emissions from fires in the *broadleaved evergreen forest* and in *mixed savanna/crop* areas (GLC2000 classes 1 and 18). Among all, GFED3 generally shows the lowest estimates as it was observed for the previous GFED2 (Kopacz et al., 2010).

In South America, the highest emissions are in the seasons March to May and June to September for the regions north and south of the Equator, respectively. All inventories agree with this trend, except VGT which appears to identify emissions from fires throughout the year with emissions also in January and February and comparable to those released during the summer months. In particular, 50% and 68% of emissions in January and February, respectively, are due to fires in the *evergreen needle-leaved forests* (GLC2000 class 4). Moreover, in the VGT inventory there is a contribution from fires in *sparse herbaceous and shrub covers* of Argentina (GLC2000 class 14) through the year which results in the anomalous emissions already highlighted in Fig. 1. These difference might be due to a reduced accuracy of the L3JRC burned area product in sparse vegetation as pointed out for other regions of the globe. Indeed, according to the L3JRC

the area burned in this land cover in 2003 is about 22% of the total area burned in South America (data not shown): the low biomass density, however, leads to a contribution in terms of emitted CO of about 5%. In this continent the lowest emissions are given by MODIS with monthly estimates always below 5 Tg of CO confirming that the underestimation of the area burned from MODIS in South America might be equally distributed during the year.

Finally, in South East Asia VGT seasonality is quite different from the other inventories and, like in South America, it depicts emissions from fires throughout the year with a minimum in December/January. On the contrary, MODIS shows a peak in January (21.25 Tg CO) due to much more extensive burning (72%) in forested areas (GLC2000 class1: *evergreen broadleaved forest*). This peak represents emissions from bushfires, which severely affected the state of Victoria in January 2003; fires started by lightning at the beginning of the month and burned for almost two months to form the largest fire in Victoria since 1939.

In the southern continental windows the apparent continuous burning throughout the year is a consequence of the fact that these windows contain the equatorial line that further splits them into northern and southern areas with alternate dry and wet seasons and therefore different timing of burning. A narrower season for the emissions can instead be observed during summer in the northern windows. Note that CO seasonality may be decoupled from seasonality of burned areas due to fires occurring in different land cover classes with different fuel loads and composition (van der Werf et al., 2006). We did not observe any systematic delay of the season peaks between the *bottom-up* approaches and the MOPITT dataset; delay which, on the contrary, was pointed out by previous studies (van der Werf et al., 2006; Pétron et al., 2004; Arellano et al., 2006).

Our results confirm finding by Generoso et al. (2003) who pointed out that global estimates within large regions can be corrected whereas the exact spatial and temporal description can be improved. In fact our analyses highlight the compensation effects hiding behind synthetic totals of emissions. Also Michel et al. (2005) compared emissions from different sources of remotely sensed burned area products over Asia and found a higher difference in terms of seasonality than in terms of total quantities.

3.3 CO emissions per land cover

Table 4 summarizes the proportion of the three broad land cover types within the continental windows: on average savanna/grassland occupy 41% of the land Earth surface, whereas forest and agriculture cover 36% and 23%, respectively. Note that these percentages are computed by taking into account only fire prone land cover types; yet the remaining classes cover a small proportion of the land surface. Table 5 reports emissions as Teragrams of CO and as percentage given by VGT, ATSR, and MODIS inventories for forest,

Table 4. Spatial distribution [10^6 km^2] and proportion [%] of the area covered by each class for the continental windows and for the globe.

Land cover	N. America		Europe		N. Asia		S. America		Africa		South East Asia		Globe	
Forest	7.67	45	3.05	33	10.10	41	8.80	46	4.08	21	3.83	25	**37.53**	**36**
Sav&Grass	7.29	43	2.33	25	9.71	39	5.46	29	11.08	58	7.52	49	**43.37**	**41**
Agriculture	2.05	12	3.87	42	5.02	20	4.70	25	4.05	21	4.15	27	**23.85**	**23**

Table 5. Contribution to the total annual CO emissions of forest, savanna/grassland and agriculture over the continental windows and the globe [Tg/y, %]. In the last column, for the globe we also provide percentage of burned area [BA%] in each class.

	N. America		Europe		N. Asia		S. America		Africa		South East Asia		Globe		
Emissions	Tg/y	%	Tg/y	%	Tg/y	%	Tg/y	%	Tg/y	%	Tg/y	%	Tg/y	%	BA %
							Forest								
VGT	260.3	18	71.7	5	499.1	35	87.0	6	106.2	7	30.1	2	1054.3	74	26
ASTR	45.4	8	5.3	1	122.8	22	63.9	12	93.9	17	20.9	4	352.3	64	19
MODIS	18.5	2	10.5	1	220.0	29	31.8	4	208.8	27	71.7	9	561.2	73	27
							Savanna and Grassland								
VGT	13.3	1	4.6	0	43.7	3	32.5	2	187.1	13	43.1	3	324.3	23	56
ATSR	2.4	0	0.8	0	10.5	2	23.0	4	101.3	19	35.0	6	173.0	32	63
MODIS	0.6	0	1.1	0	13.4	2	2.3	0	138.3	18	19.0	2	174.7	23	53
							Agriculture								
VGT	3.1	0	11.5	1	16.4	1	2.3	0	9.4	1	0.7	0	43.4	3	18
ATSR	0.3	0	1.2	0	6.2	1	6.1	1	6.4	1	2.0	0	22.2	4	18
MODIS	0.1	0	1.6	0	7.0	1	1.5	0	20.3	3	1.9	0	32.4	4	21

savanna/grassland and agriculture biomes; for the globe the percentage of burned area responsible for the emission is also shown.

More than 70% of the global CO emissions from vegetation fires in 2003 came from forests as estimated from the VGT and MODIS inventories and 64% according to ATSR whilst the area burned accounted only for between 19–27%. Note that, similar proportional contributions over the globe may hide a large difference in terms of the amount of emitted CO, such as in the case of VGT and MODIS (73–74%; 1054.3–561.2 Tg CO). In the forest biome, VGT provides the greatest estimates for all continents except Africa and South East Asia; yet we have already discussed the high uncertainty of emissions given by VGT in boreal regions. VGT estimates are significantly higher than the other two inventories in the GLC02 (*deciduous broadleaved closed forest*) and GLC05 (*deciduous needle-leaved forest*) land cover classes. MODIS estimates are the greatest in South East Asia due to the contribution in December–February (ten times greater than VGT and ATSR) of the *evergreen broadleaved forest* (GLC2000 class 1) as also observed in Fig. 2. Discarding the VGT per-

centage contribution, which might be biased by uncertainty, fires in the boreal forests of the Russian Federation are the source of 22–29% of the global CO emitted from biomass burning in 2003. The same inventories show that tropical forests in South America and Africa together are responsible of about 30% of the global annual emissions. ATSR shows that 12% of the global emissions are due to fires in South American forests whereas MODIS shows a similar contribution of forests in South East Asia.

Although between 53% and 63% of the total burned area is in savannas and grasslands, their contribution to CO emissions is in the range 23–32%; between 13% and 19% of the total emissions are from fires in Africa, which is the most important continent for global CO emissions from biomass burning in savannas. The range of estimates of total emissions from savannas and grasslands is 173.0–324.3 Tg CO with ATSR and MODIS almost identical despite a different distribution among the continents. The largest difference is seen for South American savannas where MODIS estimates are of one order of magnitude lower than the other two inventories (see also Fig. 2). Hence MODIS underestimates

not only in forest canopies but also over savannas and grasslands.

Finally, agricultural fires which account for about 20% of the total burned area, are responsible of only 3–4% of the global CO emissions. The difference in terms of Teragrams is of the same order of magnitude as in the other biomes: VGT is two fold the lowest estimate provided by the other two inventories. Although agricultural fires little contribute compared to the other two biomes globally, they might become significant at the continental scale. For example, in Europe their contribution is in the range 8–10%. For these fires, a major issue is that the majority of the burned areas are small compared to the sensor's pixel size and may therefore remain undetected. Our analyses show that, only in agricultural areas of South East Asia, ATSR and MODIS estimates are systematically greater than VGT and overall the highest estimate is given by MODIS in Africa (20.3 Tg CO).

These results confirm findings by Michel et al. (2005) who highlighted that the inter-annual difference in total amounts of CO emissions in Asia from different remotely sensed burned area products is often given by the forest classes which, with high biomass densities, greatly contribute to the total emissions. Moreover, forests more than other land covers play a key role in the global budget of reduced chemical species, such as CO, which are the product of the incomplete combustion of live biomass (see also emission factors in Mieville et al., 2010). Despite an increase in the accuracy of burned area maps, an accurate parameterization of vegetation characteristics and conditions at the time of fire occurrence is necessary.

The seasonality of CO emissions per land cover type is shown in Fig. 3. First of all, it highlights the anomalies of the seasonality given by the VGT inventory over the northern windows due to the lower reliability of the L3JRC burned area product outside the fire season (Chang and Song, 2009). All of the three broad land covers contribute to the anomalous peaks of CO emissions in spring and autumn although forests play a key role due to the greater amount of biomass involved in burning. Note that in Northern Asia the anomaly seems to be restricted to the September/October period. In agriculture regions of the northern windows CO emissions have two peaks although VGT overestimates; the most similar trend between the inventories can be observed for Northern Asia with intense emissions in May and October due to fires in permanent agriculture regions of Russia, Ukraine and Kazakhstan: here fires before planting and after harvest are a quite common land management (Korontzi et al., 2006). In Europe, where agriculture fires are important, the three inventories provide a different seasonality and only VGT well highlights the two peaks typical of managed areas (spring and autumn).

In South America the lack of seasonality of emissions from VGT shown in Fig. 2 is due to the forest class whereas over savannas the three inventories have a clear but different seasonality. It is confirmed the underestimation of MODIS burned areas in all of the three classes in this continent. In South-America ATSR estimates in agricultural lands are greater than the others and show peaks in March and September: the detailed classes contributing to these two maxima are the *shrub/grass* and *crop mosaic* (GLC2000 class 18) and *cultivated/managed* areas (GLC2000 class 16), respectively, with almost 0.7 Tg CO each.

In Africa emissions show a good agreement in seasonality with the exception of the June to August emissions due to fires in southern savannas and observed only in the VGT inventory. We believe that the seasonality provided by VGT estimates is more reliable and confirms the temporal dynamics reported by other studies (Roberts et al., 2009). Our results highlight that in Northern Africa VGT and MODIS provide estimates of the same order of magnitude (see December/January emissions) thus suggesting that underestimation by VGT might be produced by forest regions rather than savannas. In forests, MODIS overestimates emissions in January thus leading to the anomaly already highlighted in Fig. 2.

In South East Asia a good agreement between VGT and ATSR is reached for forest and between MODIS and ATSR from agricultural fires in terms of both emission amounts and seasonality.

4 Conclusions

This work compares five inventories of global CO emissions from biomass burning for the year 2003 derived from satellite data and named VGT, ATSR, MODIS, GFED3 and MOPITT. Different data and models are involved in the comparison: *bottom-up* and *top-down* approaches, active fire counts and burned area maps, different satellite sensors, common fixed broad land cover type and fuel loads based on biogeochemical model, fixed and time dependent burning efficiency. Some of the inventories (e.g. ATSR and MOPITT) might be correlated since they both use the ATSR night-time active fires; however, the independence of the datasets is not a requirement for the comparison of the inventories. Moreover, the different methods used for deriving CO estimates lead to different spatial and temporal patterns also in the case of inventories which are correlated. Despite the improvement brought by the recent and newer satellite based fire products, large uncertainty still remains in the estimation of emissions from biomass burning, which range for the year 2003 between 365 Tg CO (GFED3) and 1422 Tg CO (VGT). Globally, the VGT inventory provides the highest estimates of CO emissions whereas ATSR and GFED3 the lowest ones. The ATSR inventory might be biased by the use of night-time active fire counts, which represent a temporal sampling of the diurnal fire activity. The conservative estimates of the GFED3 might be due to the combination of lower values for the area burned and for fuel consumption. Global GFED3 estimates are lower than the previous GFED2, which was
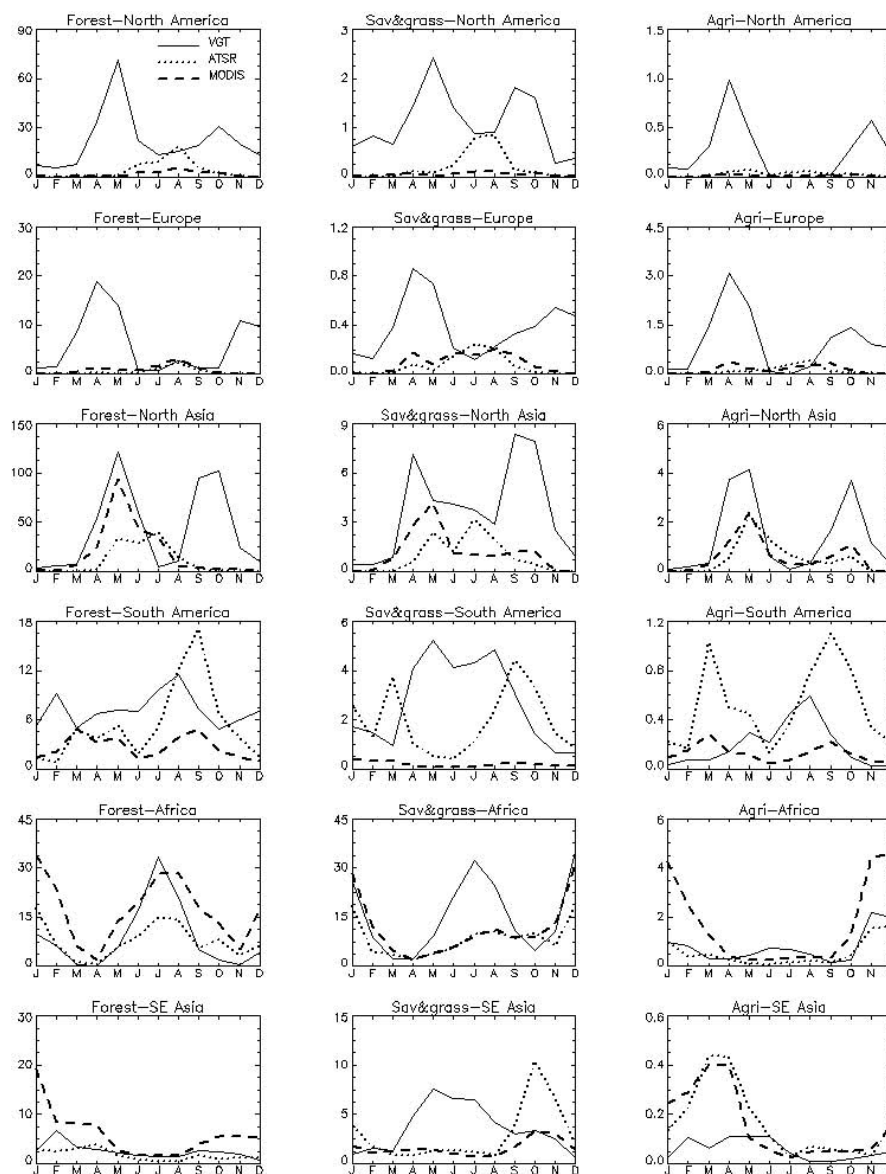
Fig. 3. Seasonality of CO emissions [Tg CO month^{-1}] for the six continental windows and the three broad land cover types (forest, savanna/grassland and agriculture).

considered to underestimate emissions especially over tropical regions. Some of the global spatial patterns typical of biomass burning are given by all inventories: boreal forest fires in central and eastern Siberia, agricultural fires in Eastern Europe and Russia and savannas burning in South America, Africa and Australia. Africa and Northern Asia are confirmed to be the most important contributors to global CO emissions from biomass burning.

The comparison of VGT, ATSR and MODIS per broad land cover types shows that forests due to the higher fuel loads and therefore fuel consumption contribute 64–74% to the global CO emissions despite accounting for *only* 19–27% of the total area burned. On the contrary, fires in sa-

vannas and grasslands, which contribute with 53–63% to the global burned area, are responsible for 23–32% of the global emissions of CO. Finally, fires related to agricultural practices account for about 20% of the total burned area but *only* 3–4% of the global CO emissions. Although at the global scale agricultural fires little contribute compared to the other two biomes, they might become significant at the continental level: in Europe their contribution is in the range 8–10%.

Even larger differences, hence uncertainty, are highlighted by the regional analysis. The VGT inventory overestimates at the northernmost latitudes with respect to the other inventories. The CV of annual totals for North America and Europe is above 145% whereas it is 88% for northern Asia. The VGT

seasonality has anomalous peaks of CO emissions in spring and autumn in North America and Europe; the other inventories agree in identifying the season peak in summer (August) although with an amount of CO which varies largely (4.8–19.1 Tg CO). Yet we believe that in some agricultural regions Europe and Russia VGT better describes practices related to burning before planting and after harvest (spring and autumn). In Northern Asia VGT overestimation is due to emission sources identified in central and eastern Siberia although a better agreement with the other inventories is achieved for the occurrence of the spring peak. The validation of the L3JRC burned area product did not provide further insights about the source of overestimation outside the fire season and therefore the use of the VGT inventory should be supervised.

A much better agreement is observed for the southern continental windows with the best correlation in terms of geographical distribution and seasonality achieved over Africa. The range for annual CO emissions in this continent is 164.7–367.4 Tg CO (CV = 31%); Africa is confirmed to be the most important contributor to global emissions by four out of five inventories. Seasonality is consistent among the inventories; the higher emissions from VGT, compared to the other inventories, in June to August are due to burning in the savannas of southern Africa. Indeed, we believe that, in this case, VGT provides the most reliable seasonality. In the MODIS inventory overestimation occurs in forest and agriculture land cover types of Africa in December/January.

In South America the VGT inventory, despite an estimate of the annual emissions consistent with the other inventories, shows an anomalous geographical location of the emission sources (i.e. savannas in Argentina rather than in Brazil). However, further analyses should be carried out to clearly identify the sources for the observed difference. In the same continent MODIS provides the lowest estimates and above all significantly low CO emissions from fires in savannas. Previous studies have pointed out that cloud cover and the loss of fires under the forest canopy might be the source of underestimation. Therefore VGT and MODIS inventories are less reliable than the other inventories over South America.

In South East Asia the range of total emissions is 52.6-92.6 Tg CO with the lowest uncertainty (CV = 24%). Among the inventories the highest estimates are given by MODIS followed by VGT. MODIS clearly depicts the high CO emissions from bushfires occurred in the Victoria state in January 2003.

Although the assessment of the accuracy of the estimates is beyond the scope of our analysis, we conclude that a large uncertainty in the global pictures of emissions from biomass burning still exists. The variability increases at the regional scale and if the geographical and seasonal distributions of the emission sources are analysed. A rate of agreement between some of the inventories at a time can be observed but it changes from region to region and it is therefore far from being global. The difference in the area burned might be the

first source of uncertainty although it impacts on the emission estimates as a function of the fuel load characteristics. There is a clear need of improving not only the accuracy of remotely sensed burned area products but also the description of vegetation characteristics and conditions especially over forests, which so greatly contribute to the CO budget. The use of the FRP for the estimation of the fuel consumption of vegetation fires is certainly a very promising approach for the future. It overcomes the limitations involved in the use of more traditional approaches, which rely on burned area mapping and on the assessment of the pre-fire fuel amounts.

Edited by: P. Middleton

References

Andreae, M. O. and Merlet, P.: Emission of trace gases and aerosols from biomass burning, Global Biogeochem. Cy., 15, 955–966, 2001.

Anyamba, A., Justice, C. O., Tucker, C. J., and Mahoney, R.: Seasonal to interannual variability of vegetation and fires at SAFARI 2000 sites inferred from advanced very high resolution radiometer time series data, J. Geophys. Res., 108(D13), 8507, doi:10.1029/2002JD002464, 2003.

Arellano, A. F., Kasibhatla, P. S., Giglio, L., van der Werf, G. R., Randerson, J. T., and Collatz, G. J.: Time-dependent inversion estimates of global biomass-burning CO emissions using Measurement of Pollution in the Troposphere (MOPITT) measurements, J. Geophys. Res., 111, D09303, doi:10.1029/2005JD006613, 2006.

Arino, O. and Plummer, S.: The Along Track Scanning Radiometer World Fire Atlas – Detection of night-time fire activity, IGBP-DIS Working Paper #23, Postdam, Germany, 2001.

Assamoi, E. and Liousse, C.: Focus on the impact of two wheel vehicles on African combustion aerosols emissions, Atmos. Environ., 44, 3985–3996, 2010.

Barbosa, P. M., Stroppiana, D., Grégoire, J.-M., and Pereira, J. C. M.: An assessment of vegetation fire in Africa (1981-1991): burned area, burned biomass, and atmospheric emissions, Global Biogeochem. Cy., 13(4), 933–950, 1999.

Bartholomé, E. and Belward, A.: GLC2000: a new approach to global land cover mapping from Earth observation data, Int. J. Remote Sens., 26(9), 1959–1977, 2005.

Bergamaschi, P., Hein, R., Heimann, M., and Crutzen, P. J.: Inversion modeling of the global CO cycle: 1. Inversion of CO mixing ratios, J. Geophys. Res., 105(D2), 1909–1927, 2000.

Bian, H., Chin, M., Kawa, S. R., Duncan, B., Arellano, A., and Kasibhatla, P.: Sensitivity of global CO simulations to uncertainties

in biomass burning sources, J. Geophys. Res., 112(D2), D23308, doi:10.1029/2006JD008376, 2007.

Boschetti, L., Eva, H. D., Brivio, P. A., and Grégoire, J.-M.: Lessons to be learned from the comparison of three satellite-derived biomass burning products, Geophys. Res. Lett., 31(21), L21501, doi:10.1029/2004GL021229, 2004.

Canadell, J. G., Raupach, M. R., and Houghton, R. A.: Anthropogenic CO_2 emissions in Africa, Biogeosciences, 6, 463–468, doi:10.5194/bg-6-463-2009, 2009.

Chang, D. and Song, Y.: Comparison of L3JRC and MODIS global burned area products from 2000 and 2007, J. Geophys. Res., 114, D16106, doi:10.1029/2008JD011361, 2009.

Chevallier, F., Fortems, A., Bousquet, P., Pison, I., Szopa, S., Devaux, M., and Hauglustaine, D. A.: African CO emissions between years 2000 and 2006 as estimated from MOPITT observations, Biogeosciences, 6, 103–111, doi:10.5194/bg-6-103-2009, 2009.

Chin, M., Ginoux, P., Kinne, S., Torres, O., Holben, B. N., Duncan, B. N., Martin, R. V., Logan, J. A., Higurashi, A., and Nakajima, T.: Tropospheric Aerosol Optical Thickness from the GOCART Model and Comparisons with Satellite and Sun Photometer Measurements, J. Atmos. Sci., 59, 461–483, 2002.

Conard, S. G., Sukhinin, A. I., Stocks, B. J., Cahoon, D. R., Davidenko, E. P., and Ivanova, G. A.: Determining effects of area burned and fire severity on carbon cycling and emissions in Siberia, Climatic Change, 55, 197–211, 2002.

Cooke, W. F., Koffi, B., and Grégoire, J. M.: Seasonality of vegetation fires in Africa from remote sensing data and application to a global chemistry model, J. Geophys. Res., 101, 21051–21065, 1996.

Crutzen, P. J. and Zimmermann, P. H.: The changing photochemistry f the troposphere, Tellus, 43AB, 136–151, 1991.

Crutzen, P. J., Heidt, L. E., Krasnec, J. P., Pollock, W. H., and Seiler, W.: Biomass burning as a source of atmospheric gases CO, H_2, N_2O, NO, CH_3CL and COS. Nature, 282, 253–256, 1979.

Dwyer, E., Pinnock, S., Grégoire, J.-M., and Pereira, J. M. C.: Global spatial and temporal distribution of vegetation fires as determined from satellite observations, Int. J. Remote Sens., 21, 1289–1302, 2000.

Edwards, D. P , Emmons, L. K., Hauglustaine, D. A., Chu, A., Gille, J. C., Kaufman, Y. J., Petron, G., Yurganov, L. N., Giglio, L., Deeter, M. N., Yudin, V., Ziskin, D. C., Warner, J., Lamarque, J. -F., Francis, G. L., Ho, S. P., Mao, D., Chen, J., Grechko, E. I., and Drummond, J. R.: Observations of carbon monoxide and aerosols from the Terra satellite: Northern Hemisphere variability, J. Geophys. Res., 109, D24202, doi:10.1029/2004JD004727, 2004.

Friedli, H. R., Arellano, A. F., Cinnirella, S., and Pirrone, N.: Initial estimates of mercury emissions to the atmosphere from global biomass burning, Environ. Sci. Technol., 43, 3507–3513, 2009.

Generoso, S., Bréon, F.-M., Balkanski, Y., Boucher, O., and Schulz, M.: Improving the seasonal cycle and interannual variations of biomass burning aerosol sources, Atmos. Chem. Phys., 3, 1211–1222, doi:10.5194/acp-3-1211-2003, 2003.

Giglio, L., van der Werf, G. R., Randerson, J. T., Collatz, G. J., and Kasibhatla, P.: Global estimation of burned area using MODIS active fire observations, Atmos. Chem. Phys., 6, 957–974, doi:10.5194/acp-6-957-2006, 2006.

Giglio, L., Loboda, T., Roy, D. P., Quayle, B., and Justice, C. O.: An active-fire based burned area mapping algorithm for the MODIS sensor, Remote Sens. Environ., 113, 408–420, doi:10.1016/j.rse.2008.10.006, 2009.

Giglio, L., Randerson, J. T., van der Werf, G. R., Kasibhatla, P. S., Collatz, G. J., Morton, D. C., and DeFries, R. S.: Assessing variability and long-term trends in burned area by merging multiple satellite fire products, Biogeosciences, 7, 1171–1186, doi:10.5194/bg-7-1171-2010, 2010.

Grégoire, J.-M., Tansey, K., and Silva, J. M. N.: The GBA2000 initiative: Developing a global burned area database from SPOT-VEGETATION imagery, Int. J. Remote Sens., 24(6), 1369–1376, 2003.

Hély, C., Dowty, P. R., Alleaume, S., Caylor, K. K., Korontzi, S., Swap, R. J., Shugart, H. H., and Justice, C. O.: Regional fuel load for two climatically contrasting years in southern Africa, J. Geophys. Res., 108(D13), 8475, doi:10.1029/2002JD002341, 2003.

Hobbs, P. V., Reid, J. S., Kotchenruther, R. A., Ferek, R. J., and Weiss, R.: Direct Radiative forcing by smoke from biomass burning, Science, 275, 1776–1778, 1997.

Horowitz, L., Walters, S., Mauzerall, D., Emmons, L., Rasch, P., Granier, C., Tie, X., Lamarque, J.-F., Schultz, M., Tyndall, G., Orlando, J., and Brasseur, G.: A global simulation of tropospheric ozone and related tracers: Description and evaluation of MOZART, version 2, J. Geophys. Res., 108, 4784, doi:10.1029/2002JD002853, 2003.

Innes, J. L., Beniston, M., and Verstraete, M. M. (Eds.): Biomass burning & its inter-relations with the climate system, The Netherlands: Kluwer Academic Publishers, 2000.

IPCC-Intergovernmental Panel on Climate Change 2001, Climate Change 2001, The scientific basis, available at: http://www.ipcc.ch/ipccreports/tar/wg1/index.htm, 2001.

IPCC-Intergovernmental Panel on Climate Change 2007, Climate Change 2007, The physical science basis, http://www.ipcc.ch/ipccreports/ar4-wg1.htm, 2007.

Jain, A. K.: Global estimation of CO emissions using three sets of satellite data for burned area, Atmos. Environ., 41, 6931–6940, 2007.

Justice, C. O., Giglio, L., Korontzi, S., Owens, J., Morisette, J., Roy, D., Descloitres, J., Alleaume, S., Petitcolin, F., and Kaufman, T.: The MODIS fire products, Remote Sens. Environ., 83, 244–262, 2002.

Konare, A., Liousse, C., Guillaume, B., Solmon, F., Assamoi, P., Rosset, R., Gregoire, J. M., and Giorgi, F.: Combustion particulate emissions in Africa: regional climate modeling and validation, Atmos. Chem. Phys. Discuss., 8, 6653–6681, doi:10.5194/acpd-8-6653-2008, 2008.

Kopacz, M., Jacob, D. J., Fisher, J. A., Logan, J. A., Zhang, L., Megretskaia, I. A., Yantosca, R. M., Singh, K., Henze, D. K., Burrows, J. P., Buchwitz, M., Khlystova, I., McMillan, W. W., Gille, J. C., Edwards, D. P., Eldering, A., Thouret, V., and Nedelec, P.: Global estimates of CO sources with high resolution by adjoint inversion of multiple satellite datasets (MOPITT, AIRS, SCIAMACHY, TES), Atmos. Chem. Phys., 10, 855–876, doi:10.5194/acp-10-855-2010, 2010.

Korontzi, S., McCarty, J., Loboda, T., Kumar, S., and Justice, C.: Global disitrubtion of agricultural fires in croplands from 3 years of Moderate Resolution Imaging Spectroradiometer (MODIS) data, Global Biogeochem. Cy., 20(2), G2021,

doi:10.1029/2005GB002529, 2006.

Langenfelds, R. L., Francey, R. J., Pak, B. C., Steele, L. P., Lloyd, J., Trudinger, C. M., and Allison, C. E.: Interannual growth rate variations of atmospheric CO_2 and its d13C, H_2, CH_4 and CO between 1992 and 1999 linked to biomass burning, Global Biogeochem. Cy., 16, 1048, doi:10.1029/2001GB001466, 2002.

Langmann, B., Duncan, B., Textor, C., Trentmann, J., and van der Werf, G. R.: Vegetation fire emissions and their impact on air pollution and climate, Atmos. Environ, 43, 107–116, 2009.

Liousse, C., Penner, J. E., Walton, J. J., Eddleman, H., Chuang, C., and Cachier, H.: Modelling Biomass burning aerosols, in: Biomass Burning and Global Change, edited by: dir. Levine J. S., MIT Press (Cambridge), 492–508, 1996.

Liousse, C., Andreae, M. O., Artaxo, P., Barbosa, P., Cachier, H., Grégoire, J. M., Hobbs, P., Lavoué, D., Mouillot, F., Penner, J., and Scholes, M.: Deriving Global Quantitative Estimates for Spatial and Temporal Distributions of Biomass Burning Emissions, in: Emissions of Atmospheric Trace Compounds, edited by: Granier, C., Artaxo, P., and Reeves, C., Kluwer Academic Publishers, Dordrecht, The Netherlands, 544 pp., 2004.

Liousse, C., Guillaume, B., Grégoire, J.M., Mallet, M., Galy, C., Poirson, A., Solmon, F., Pont, V., Mariscal, A., Dungal, L., Rosset, R., Yoboué, V., Bedou, X., Serça, D., Konaré, A., Granier, C., and Mieville, A.: African Aerosols Modeling during the EOP-AMMA campaign with updated biomass burning emission inventories, to be submitted to Atmos. Chem. Phys. Discuss., 2010.

Liu, J., Drummond, J. R., Li, Q., Gille, J. C., and Ziskin, D. C.: Satellite mapping of CO emission from forest fires in Northwest America using MOPITT measurements, Remote Sens. Environ., 95, 502–516, 2005.

Manning, M. R., Brenninkmeijer, C. A. M., and Allan, W.: The atmospheric carbon monoxide budget of the southern hemisphere: implication of $^{13}C/^{12}C$ measurements, J. Geophys. Res., 102, 10673–10682, 1997.

Mieville, A., Granier, C., Liousse, C., Guillaume, B., Mouillot, F., Lamarque, J.-F., Grégoire, J.-M., and Pétron, G.: Emissions of gases and particles from biomass burning during the 20th century using satellite data and an historical reconstruction, Atmos. Environ., 44, 1469–1477, 2010.

Michel, C., Liousse, C., Grégoire, J.-M., Tansey, K., Carmichael, G. R., and Woo, J.-H.: Biomass burning emission inventory from burn area data given by the SPOT-VEGETATION system in the fram of TRACE-P and ACE-Asia campaigns, J. Geophys. Res., 110, D09304, doi:10.1029/2004JD005461, 2005.

Mollicone, D., Eva, H., and Achard, F.: Human role in Russian wild fires, Nature, 440, 436–437, 2006.

Mota, B. W., Pereira, J. M. C., Oom, D., Vasconcelos, M. J. P., and Schultz, M.: Screening the ESA ATSR-2 World Fire Atlas (1997–2002), Atmos. Chem. Phys. Discuss., 5, 4641–4677, doi:10.5194/acpd-5-4641-2005, 2005.

NASA/University of Maryland: MODIS Hotspot / Active Fire Detections. Data set. MODIS Rapid Response Project, NASA/GSFC [producer], University of Maryland, Fire Information for Resource Management System [distributors], available at: http://maps.geog.umd.edu/firms/firedata.htm (last access: December 2010), 2002.

Novelli, P. C., Masarie, K. A., Lang, P. M., Hall, B. D., Myers, R. C., and Elkins, J. W.: Reanalysis of tropospheric CO trends:

Effects of the 1997–1998 wildfires, J. Geophys. Res.-Atmos., 108(D15), 4464, doi:10.1029/2002JD003031, 2003.

Olivier, J. G. J. and Berdowski J. J. M.: Global emissions sources and sinks, in: The Climate System, edited by: Berdowski, J., Guicherit, R., and Heij, B. J., A. A. Balkema, Brookfield, Vt., 33–78, 2001.

Pétron, G., Granier, C., Khattatov, B., Larmarque, J.-F., Yudin, V., Muller, J.-F., and Gille, J.: Inverse modeling of carbon monoxide surface emissions using CMDL network observations, J. Geophys. Res., 107(D24), 4762, doi:10.1029/2001JD002049, 2002.

Pétron, G., Granier, C., Khattatov, B., Yudin, V., Lamarque, J.-F., Emmons, L., Gille, J., and Edwards, D. P.: Monthly CO surface sources inventory based on the 2000–2001 MOPITT satellite data, Geophys. Res. Lett., 31, L21107, doi:10.1029/2004GL020560, 2004.

Podgorny, I. A., Li, F., and Rammanathan, V.: Large aerosol radiative forcing due to the 1997 Indonesian forest fire, Geophys. Res. Lett., 30, GL015979, doi:10.1029/2002GL015979, 2003.

Reid, J. S., Koppmann, R., Eck, T. F., and Eleuterio, D. P.: A review of biomass burning emissions part II: intensive physical properties of biomass burning particles, Atmos. Chem. Phys., 5, 799–825, doi:10.5194/acp-5-799-2005, 2005.

Roberts, G., Wooster, M. J., and Lagoudakis, E.: Annual and diurnal african biomass burning temporal dynamics, Biogeosciences, 6, 849–866, doi:10.5194/bg-6-849-2009, 2009.

Seiler, W. and Crutzen, P. J.: Estimate of gross and net fluxes of carbon between the biosphere and the atmosphere from biomass burning, Climate Change, 2, 207–247, 1980.

Schultz, M. G.: On the use of ATSR fire count data to estimate the seasonal and interannual variability of vegetation fire emissions, Atmos. Chem. Phys., 2, 387–395, doi:10.5194/acp-2-387-2002, 2002.

Stroppiana, D., Brivio, P. A., and Grégoire, J.-M.: Modelling the impact of vegetation fires, detected from NOAA-AVHRR data, on tropospheric chemistry in tropical Africa. In Biomass burning & its inter-relations with the climate system, The Netherlands: Kluwer Academic Publishers, 193–213, 2000.

Tansey, K., Grégoire, J. M., Stroppiana, D., Sousa, A., Silva, J., Pereira, J. M. C., Boschetti, L., Maggi, M., Brivio, P. A., Fraser, R., Flasse, S., Ershov, D., Binaghi, E., Graetz, D., and Peduzzi, P.: Vegetation burning in the year 2000: Global burned area estimates from SPOT vegetation data, J. Geophys. Res., 109, D14S03, doi:10.1029/2003JD003598, 2004.

Tansey, K., Grégoire, J. M., Defourny, P., Leigh, R., Pekel, J. F., Van Bogaert, E., and Bartholomè, E.: A new, global, multi-annual (2000–2007) burnt area product at 1 km resolution, Geophys. Res. Lett., 35, L01401, doi:10.1029/2007GL031567, 2008.

van der Werf, G. R., Randerson, J. T., Collatz, G. J., Giglio, L., Kasibhatla, P. S., Arellano, A. F., Olsen, S. C., and Kasichke, E.: Continental-scale partitioning of fire emissions during the 1997 to 2001 El Nino/La Nina period, Science, 303, 73–76, 2004.

van der Werf, G. R., Randerson, J. T., Giglio, L., Collatz, G. J., Kasibhatla, P. S., and Arellano Jr., A. F.: Interannual variability in global biomass burning emissions from 1997 to 2004, Atmos. Chem. Phys., 6, 3423–3441, doi:10.5194/acp-6-3423-2006, 2006.

van der Werf, G. R., Randerson, J. T., Giglio, L., Collatz, G. J., Mu, M., Kasibhatla, P. S., Morton, D. C., DeFries, R. S., Jin, Y., and van Leeuwen, T. T.: Global fire emissions and the contribution of

deforestation, savanna, forest, agricultural, and peat fires (1997–2009), Atmos. Chem. Phys., 10, 11707–11735, doi:10.5194/acp-10-11707-2010, 2010.

Westerling, A. L., Hidalgo, H. G., Cayan, D. R., and Swetnam, T. W.: Warming and earlier spring increase western U.S. forest wildfire activity, Science, 313, 940–943, doi:10.1126/science.1128834, 2006.

Williams, C. A., Hanan, N. P., Neff, J. C., Scholes, R. J., Berry, J. A., Denning, A. S., and Baker, D. F.: Africa and the global carbon cycle, Carbon Balance and Management, 2(3), doi:10.1186/1750-0680-2-3, 2007.

Wooster, M. J., Roberts, G., Perry, G. L. W., and Kaufman, Y. J.: Retrieval of biomass combustion rates and totals from fire radiative power observations: FRP derivation and calibration relationships between biomass consumption and fire radiative energy release, J. Geophys. Res., 110, D24311, doi:10.1029/2005JD006318, 2005.

Yan, X., Ohara, T., and Akimoto, H.: Bottom-up estimate of biomass burning in mainland China, Atmos. Environ., 40, 5262–5273, 2006.

Yurganov, L. N., Duchatelet, P., Dzhola, A. V., Edwards, D. P., Hase, F., Kramer, I., Mahieu, E., Mellqvist, J., Notholt, J., Novelli, P. C., Rockmann, A., Scheel, H. E., Schneider, M., Schulz, A., Strandberg, A., Sussmann, R., Tanimoto, H., Velazco, V., Drummond, J. R., and Gille, J. C.: Increased Northern Hemispheric carbon monoxide burden in the troposphere in 2002 and 2003 detected from the ground and from space, Atmos. Chem. Phys., 5, 563–573, doi:10.5194/acp-5-563-2005, 2005.